RSC Applied Interfaces

ROYAL SOCIETY OF CHEMISTRY

PAPER

View Article Online
View Journal | View Issue

Check for updates

Cite this: *RSC Appl. Interfaces*, 2025, **2**, 1031

Carbon fibres as electrodes for the recovery of nickel from industrial wastewater†

Annu Pandey,[a] Anton Bjurström, [abc] Björn K. Birdsong,[a] Ronald Arvidsson,[d] Paya Rabii Dezfoli,[a] Kåre Tjus, [e] Sofia Andrée,[f] Stefan Sädbom,[g] Anders Björk *[e] and Richard T. Olsson *[ab]

This study presents an innovative approach to the recovery of nickel from industrial wastewater using cost-effective carbon fiber electrodes, aiming to provide a sustainable and scalable solution for industrial effluent management. Carbon fibers offer unique benefits in electrochemical recovery processes due to their high surface area, excellent conductivity, mechanical durability, and compatibility with low-cost production. The optimized conditions, including a deposition potential of 4 V, pH 3.5, and temperature of 60 °C, achieved a high nickel recovery efficiency of 90%, with minimal energy consumption at 3 kW h per kilogram of nickel. This efficiency was verified through Scanning Electron Microscopy (SEM) and Energy Dispersive X-ray (EDX) analyses, which revealed uniform and dense nickel coatings on the carbon fibers, even under continuous operation. Fourier Transform Infrared Spectroscopy (FTIR) and X-ray diffraction (XRD) confirmed successful nickel deposition and modifications to the carbon fiber surface chemistry, enhancing the adsorption and reduction of nickel ions. Using carbon fiber electrodes in this process addresses several limitations in traditional electrode materials by reducing costs, improving scalability, and supporting continuous, large-scale nickel recovery. This method offers a viable alternative to conventional electrochemical metal recovery and contributes to circular resource utilization by recycling valuable metals from wastewater. With regulatory pressures increasing around heavy metal discharge limits, this carbon fiber-based electrodeposition process presents a highly promising solution for industrial wastewater treatment, combining environmental sustainability with economic feasibility.

Received 7th December 2024,
Accepted 23rd April 2025

DOI: 10.1039/d4lf00409d

rsc.li/RSCApplInter

Open Access Article. Published on 24 balandžio 2025. Downloaded on 2026-01-26 03:41:21.
This article is licensed under a Creative Commons Attribution 3.0 Unported Licence.

1. Introduction

The extraction processes generate substantial volumes of wastewater containing valuable industrial metals such as zinc (Zn), lead (Pb), cadmium (Cd), and nickel (Ni).[1–4] Among heavy metals, nickel stands out due to its extensive industrial use and value as a raw material. Nickel is commonly utilized in high-value industrial processes, including metal plating, electroplating, alloy production, and chemical manufacturing, leading to elevated levels of nickel in industrial wastewater. High nickel concentrations in discharged wastewater can result in severe environmental pollution and health concerns for exposed individuals.[5–12] The Ni(II) is readily available and more toxic in cationic form than its complexes. Although Ni(III) may be more toxic on a molecular level due to its oxidative potential, Ni(II) is of greater concern in environmental and public health contexts because it is more stable and more likely to cause chronic exposure. As a result, most toxicological studies and environmental regulations focus on Ni(II).[13,14] Managing nickel-contaminated wastewater is crucial for mitigating environmental damage and safeguarding human health.[15–19] The European Union's stringent requirement for Ni(II) discharge is set at 0.03 mg L^{-1} (2010/75/EU).[20] Under the EU Water Framework Directive, the maximum allowable concentration of 34 μg L^{-1} reflects its potential to harm aquatic life even at low levels. For soil, acceptable concentrations vary depending on land use, but general thresholds for agricultural land range between 30 to 75 mg kg^{-1} of nickel content. These values highlight the importance of monitoring and regulating nickel emissions to

[a] *School of Chemical Science and Engineering, Fibre and Polymer Technology – Polymeric Materials, KTH – Royal Institute of Technology, Teknikringen 56-58, 100 44 Stockholm, Sweden. E-mail: rols@kth.se*
[b] *Wallenberg Initiative Materials Science for Sustainability, Department of Fibre and Polymer Technology, KTH Royal Institute of Technology, Stockholm, SE-106 91 Stockholm, Sweden*
[c] *NKT HV Cables, Technology Consulting, SE-721 78 Västerås, Sweden*
[d] *Geological Survey of Sweden, Villavägen 18, SE-752 36 Uppsala, Sweden*
[e] *IVL Swedish Environmental Research Institute, Stockholm, Sweden. E-mail: anders.bjork@ivl.se*
[f] *Tube R & D, Alleima, SE-81 181 Sandviken, Sweden*
[g] *Senior Exploration Geologist/Chairman, Lovisagruvan AB, Box 250, SE-711 04 Storå, Sweden*

† Electronic supplementary information (ESI) available. See DOI: https://doi.org/10.1039/d4lf00409d

© 2025 The Author(s). Published by the Royal Society of Chemistry

Open Access Article. Published on 24 balandžio 2025. Downloaded on 2026-01-26 03:41:21.
This article is licensed under a Creative Commons Attribution 3.0 Unported Licence.

minimize ecological risks and protect public health.[21,22] Stringent regulations and enforcement mechanisms are therefore vital in ensuring compliance with environmental standards and promoting sustainable mining practices.[23] Various treatment methods, including sedimentation, chemical precipitation, membrane separation, ion exchange, and advanced oxidation processes, remove heavy metals from wastewater before discharge.[24,25] Strategies such as containment ponds, liners, and regular monitoring are implemented to prevent leakage of contaminated water into surrounding ecosystems.[26] Despite these efforts, challenges persist in effectively recovering nickel from wastewater, including high treatment costs and complexity in treating multiple contaminants simultaneously. Therefore, continual technological advancements are necessary to improve treatment efficiency, including the additional recovery of valuable metals such as Zn, Pb, and Cd.[16–19,27–29]

Electrochemical methods, particularly electrolysis and electrochemical deposition (electroplating), present promising solutions for nickel recovery. These methods are economically viable and eco-friendly and are widely used to develop corrosion-preventing coatings and as pretreatments for further metallic depositions. However, optimizing large-scale electrochemical reactors is essential, with the choice of electrodes playing a pivotal role in determining the efficiency and quality of nickel recovery.[30–36] Inexpensive carbon fibers emerge as innovative electrode materials for nickel recovery from treated wastewater *via* electrodeposition. Their high conductivity, durability, and flexibility make them ideal for this application, providing high surface areas and active sites for nickel ion adsorption and reduction from wastewater solutions, offering a cost-effective and efficient alternative to traditional electrodes.[32,37–39]

This study demonstrates the effectiveness of conductive carbon fibers as high-performance electrodes for nickel recovery from wastewater. A 90% recovery efficiency of nickel at the low potential of 4 V with minimal energy consumption (3 kW h per kg of nickel) demonstrates significant potential for scalability within sustainable resource recovery. A detailed characterization of the nature of the carbon fibers before and after electrodeposition using high-resolution microscopy, FTIR/UV Spectroscopy, and X-ray diffraction is presented. Further refinement of this approach will pave the way for broader application in wastewater treatment, contributing to more efficient, cost-effective, and eco-friendly solutions within industrial effluent management.

2. Experimental

2.1 Chemicals and materials

Nickel sulfate hexahydrate ($NiSO_4{\cdot}6H_2O$, ≥98%), sodium sulfate (Na_2SO_4, ≥99%), sulphuric acid (H_2SO_4, ≥98%), and sodium hydroxide (NaOH, ≥95%) were purchased from Sigma Aldrich. The boric acid (H_3BO_3, ≥99%) was brought from Alfa Aesar. The concentration of nickel salts in all sample solutions was 0.050 M, corresponding to a lower nickel concentration, which helps evaluate the electrodeposition characteristics. Polyacrylonitrile (PAN) based carbon fiber and platinum wire were obtained from PYROFIL™ TOW (TR 30S 3L, A2), Japan, and Sigma Aldrich, Sweden, respectively. True wastewater from industrial partners was analyzed and observed as containing Ni^{2+} (mg L^{-1}), $H_2PO_2^-$ (mg L^{-1}), and other co-ions like zinc (Zn^{2+}), lead (Pb^{2+}), and cadmium (Cd^{2+}), and used as a benchmark in concentration value selections during the studies.

2.2 Experimental setup and procedure

The electrodeposition experiments were carried out in an electrolytic cell of cylindrical shape with dimensions 105 × 50 × 60 mm. The synthetic (simulated) wastewater of 100 ml was prepared by dissolving the exact quantity of nickel sulfate in deionized Milli-Q water. The initial pH value of the sample solution was adjusted with H_2SO_4 or NaOH to adjust the pH of the starting solutions to the pH values required for the study. Aliquots were taken regularly to measure and characterize the stock solutions during the electrodeposition experiments. An image of the entire setup as a single-chambered electrolytic cell connected to the DC power supply is shown in Fig. 1. The power supply was connected to the carbon fiber at the cathode and to the platinum wire at the anode. The electrolytical cell was used in potentiostatic mode with constant potential applied throughout the evaluated process. The recovery rate and energy consumption were calculated by using the following formulas:

$$\text{Recovery efficiency (RE)} = (C_o - C)/C_o \times 100\% \quad (1)$$

where C_o is the initial amount of nickel in the solution (mg L^{-1}), C_e is the final concentration of nickel in the solution (mg L^{-1}), and RE is the recovery efficiency. Eqn (2) was used to calculate the energy consumption during the entire electrodeposition process to predict the system's economic nature in the recovery process.

$$W\,(\text{kW h g}^{-1}) = (U \times I + P) \times t/\Delta X \times 1000 \quad (2)$$

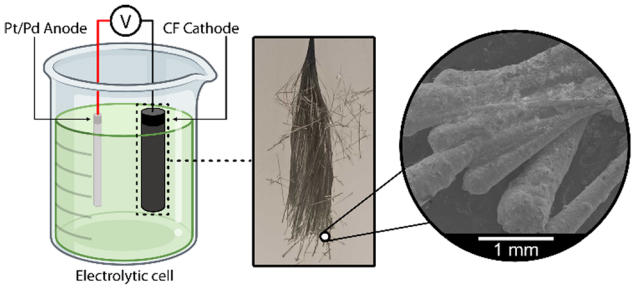

Fig. 1 Schematic of the single-chamber electrolytic cell setup, illustrating the configuration with a DC power supply connected to the carbon fiber and cathode and platinum wire as anode.

© 2025 The Author(s). Published by the Royal Society of Chemistry

Open Access Article. Published on 24 balandžio 2025. Downloaded on 2026-01-26 03:41:21.
This article is licensed under a Creative Commons Attribution 3.0 Unported Licence.

U, *I*, and *P* are the voltage (V), current intensity (A), and reaction time in hours, respectively. *P* is the power of the magnetic stirring and heating apparatus (10 W), ΔX: the recovery amount of Ni ions (mg).

Removal of polymeric carbon fiber coating (sizing). A length of approximately 1 m of carbon fibers was taken and connected to a variable autotransformer (METREL HSN0203, power: 1.82 kVA). One end was connected to the positive terminal and the other to the negative terminal. To obtain a polymer-free surface of carbon fibers, a shock heat treatment up to *ca.* 750–850 °C for 10 s was applied to the fibers by rapidly increasing the potential over the fibers filaments until the surface sizing agents were observed to be burnt and the fibers uniformly glowed with orange color. The coating of used carbon fibers was a thin layer of epoxide according to the data manufacturer sheet. This was also confirmed in this study by boiling the fibers in acetone and confirming the hydrocarbon functional coating presence in the wet acetone by Infrared spectroscopy. The complete removal was ensured by high voltage exposure to the extent that the carbon fibers started to glow with strong yellow-orange emitted light. At this state, complete degradation of the coating was evident at the temperature of 480 °C; thereafter, no additional mass loss was observed. The corresponding TGA plots have been included in the ESI,† Fig. S1.[40]

2.3 Characterization

Scanning Electron Microscopy (SEM). The morphological and chemical composition of deposits on carbon fibers were investigated using a scanning electron microscope (SEM, Hitachi SEM S-4800, Japan) equipped with an energy dispersive spectroscopy detector (EDS, X-Max 80 SDD EDS detector from Oxford Instruments, UK).

Fourier Transform Infrared Spectrophotometer (FTIR). The Perkin Elmer Spectrum 100 FT-IR spectrometer was employed to obtain infrared spectra of both nickel-deposited and non-deposited carbon fibers within the range 400 to 4000 cm^{-1}.

X-Ray Diffraction Spectroscopy (XRD). The phase composition of the nickel deposits on the carbon fibers was analyzed using X-ray powder diffraction (PANalytical X'Pert Pro X-Ray Diffractometer) with the following set-up: Cu Kα radiation (λ = 0.154 nm), 45 kV and 40 mA working current scanning from 5 °C to 70 °C at a speed of 5 °C min^{-1}.

UV-Visible Spectroscopy (UV). The amount of nickel recovered *via* electrodeposition was determined by comparing the amount of the nickel before and after the deposition process from the standard sample in the cell. Both quantities were measured using UV-vis spectroscopy (UV-2550, Shimadzu, with the cell path length equal to 10 mm).

3. Results and discussion

3.1 High-resolution microscopy of the uncoated and nickel-coated carbon fibers with surface composition analysis (EDX)

SEM analyses were performed to investigate the electrodeposited nickel film formation and its surface morphologies. The analyses were performed before and after the nickel electrodeposition at an optimal pH of 3.5 (see section 3.8). Fig. 2a shows the uncoated carbon fibers appearing smooth with well-defined longitudinal striations along the fiber axis, which stemmed from the fiber manufacturing process. The fibers are randomly oriented and mostly separated from one another on the sample holder, confirming that the polymeric coating had been successfully removed by the high-voltage treatment method. Also, minimal visible surface defects suggested a clean and intact fiber surface after removing the coating. In Fig. 2b, the nickel coating is evident on the carbon fibers, creating a textured surface on the fibers. The coating was continuous along the fibers but varied in thickness and the particle size distribution along the fibers. The more detailed SEM images confirmed the presence of agglomerate structures of nickel deposits on the outer surfaces of the carbon fiber filament bundles, consisting of the *ca.* 3000 filaments with an average thickness of *ca.* 7–8 micrometers, see Fig. 2c. This was

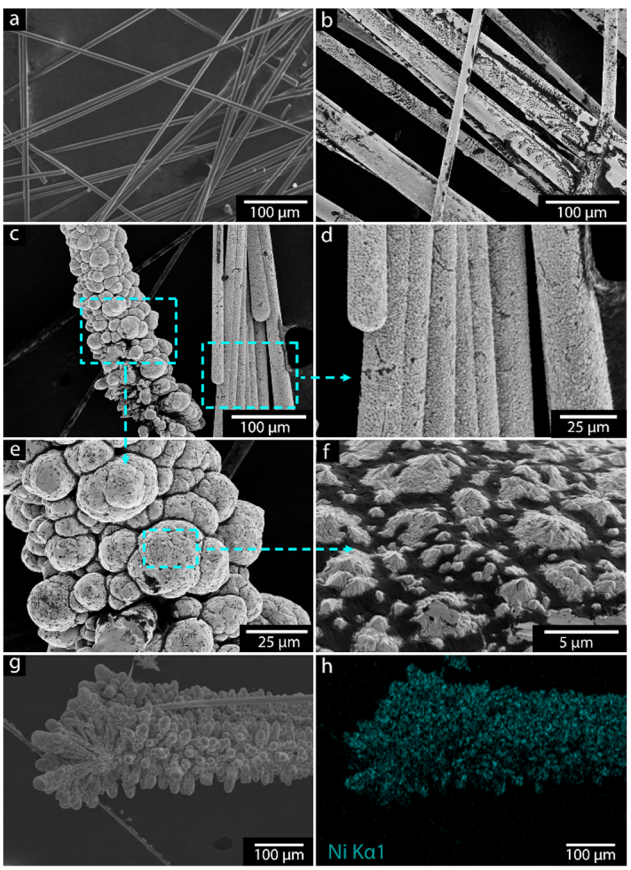

Fig. 2 a. Micrographs of carbon fiber surface before electrodeposition. b. Carbon fibers coated with nickel. c. High magnification of the nickel-coated fibers with coherent uniform coating along the filaments, with intensified deposition occurring in some areas. d. Small cracks in deposited nickel surface. e. High magnification of rough particle-shaped nickel deposits providing nucleation sites for further growth, f. High magnification of nickel deposits showing irregular polygonal shapes. g and h. EDS mapping of nickel-coated carbon fibers.

Open Access Article. Published on 24 balandžio 2025. Downloaded on 2026-01-26 03:41:21.
This article is licensed under a Creative Commons Attribution 3.0 Unported Licence.

interpreted as a result caused by the intensified electrical field strength (Fig. 2c) at local positions in the reactor vessel, causing some morphological differences in the deposited nickel. The dual morphology observed in Fig. 2c, agglomerated structures on the left and rod-like formations on the right, reflects non-uniform nickel nucleation and growth on the carbon fibre surface. The agglomerates likely arise from higher nucleation densities at surface defects, promoting isotropic growth and particle clustering, while the rod-like structures suggest anisotropic growth driven by local electric field variations. Such morphological diversity is commonly linked to substrate heterogeneity and localized electrochemical conditions. Future work will involve modelling electric field gradients to better control and optimize deposition uniformity. On the more uniformly nickel-covered filaments (Fig. 2d), cracks could be observed, suggesting internal coating stress during nickel deposition or the handling of the fibers. The surface morphology also showed larger spherical nickel particles impinging on the carbon fibers' surface, as shown in Fig. 2e. Fig. 2e also highlights the mixed particle sizes in the rough texture of the nickel surface coating; smaller nickel clusters between larger particles had been formed, suggesting secondary nucleation had occurred or incomplete coalescence during the deposition process. A more magnified view at the surface of the particles (Fig. 2f) reveals irregular polygonal shapes visible on the surface of the already coated materials, indicating a preferential deposition and further orientation crystallographic growth preference towards already formed nickel surfaces.

Fig. 2g and h show the elemental mapping of the nickel-coated carbon fibers. The bright blue color in the energy-dispersive X-ray (EDS) analysis confirmed the presence of pure nickel on the surface. The results also suggest that some nickel oxides may have deposited on the surface of carbon fibers.

Table 1 shows the elemental analysis of the nickel electrodeposits, with the relative contents of nickel to oxygen shown in column 3 for the different chemical pH conditions (Table 1). The nickel content varied based on pH, and a clear trend was observed with a more effective deposition occurring at pH 1.5 to 3.5, with deposited nickel contents >30 wt%. The lower oxygen contents observed at these lower pH values also indicated that predominantly pure metallic nickel had formed. At lower pH, the reduction potential for Ni^{2+}/Ni is more favorable, which leads to a more efficient deposition of nickel with less oxygen incorporation. In comparison, at the higher pH values, the overpotential for hydrogen evolution increases, potentially leading to more competition between hydrogen evolution and nickel deposition, which increases the incorporation of oxygen (as hydroxides or oxides).

Table 1 EDS elemental mapping of electrodeposited carbon fiber, also showing the relative ratio for the nickel to oxygen, demonstrating that it highly depends on the electrode solution pH

pH	Nickel (weight%)	Oxygen (weight%)	Actual wt of Ni recovered (g)
0.5	4.7	16.7	0.566
1.5	28.2	14.5	0.725
2.5	30.6	9.7	1.298
3.5	31.0	18.0	1.300
4.5	21.2	25.1	1.070
5.5	0.6	19.1	1.139

In summary, the SEM results demonstrate that the electrodeposition process successfully recovers nickel on the carbon fibers. The electrodeposition process on carbon fibers involves an initial nucleation phase where nickel atoms deposit and form nuclei uniformly across the fiber surface. The high nucleation density observed in the SEM micrographs indicates a well-controlled process, leading to a fine-grained and coherent nickel coating. However, irregular growth patterns and surface cracks highlighted the complexities of managing growth dynamics and stress factors during deposition. The EDS mapping further confirmed the presence and distribution of the nickel on the fibers. Optimization of deposition parameters such as electrolyte composition, potential, and deposition time was crucial to facilitate nucleation uniformity and minimize defects, thereby enhancing the overall quality of recovered nickel on carbon fibers.

3.2 FTIR analysis of electrodeposited carbon fibers

The FTIR spectra of the carbon fibers before and after coating are depicted in Fig. 3a and b. The spectrum of the pure, unmodified carbon fiber showed low absorbance across all wavenumbers, which is due to the absence or low intensity of oxygen-containing groups such as hydroxyl (–OH), carbonyl (C═O), and carboxyl (–COOH), which are known to facilitate metal ion adsorption and enhance electrochemical interactions. After the electrodeposition, the nickel-coated carbon fibers (Ni/CF) spectrum showed multiple distinct peaks with different absorbance values, reflecting the presence of functional groups and bonds introduced by the nickel-coating process. The peaks at ~3469 cm^{-1} and ~3141 cm^{-1} indicated O–H stretching vibrations associated with hydroxyl groups.[41] The absorbance at around ~2829 cm^{-1} corresponded to C–H stretching vibrations, indicative of alkane groups.[41] The peak at 1663 cm^{-1} is characteristic of C═O stretching vibrations, typically found in carbonyl groups.[41] A peak with the presence at 1663 cm^{-1} suggested that the nickel coating process introduced more hydroxyl functional groups on the carbon fiber surface.[41] Another peak at 1082 cm^{-1} corresponded to C–O stretching vibrations, which can be associated with ethers, alcohols, or esters.[41] The FTIR spectra revealed that nickel coating substantially modified the surface chemistry of carbon fibers, which was consistent with the formation of an inorganic metal oxide/metal phase on the surface of the carbon fibers. However, many of the peaks were related to the carbon functionalities that formed due to the extensive oxidation of

© 2025 The Author(s). Published by the Royal Society of Chemistry

Open Access Article. Published on 24 balandžio 2025. Downloaded on 2026-01-26 03:41:21.
This article is licensed under a Creative Commons Attribution 3.0 Unported Licence.

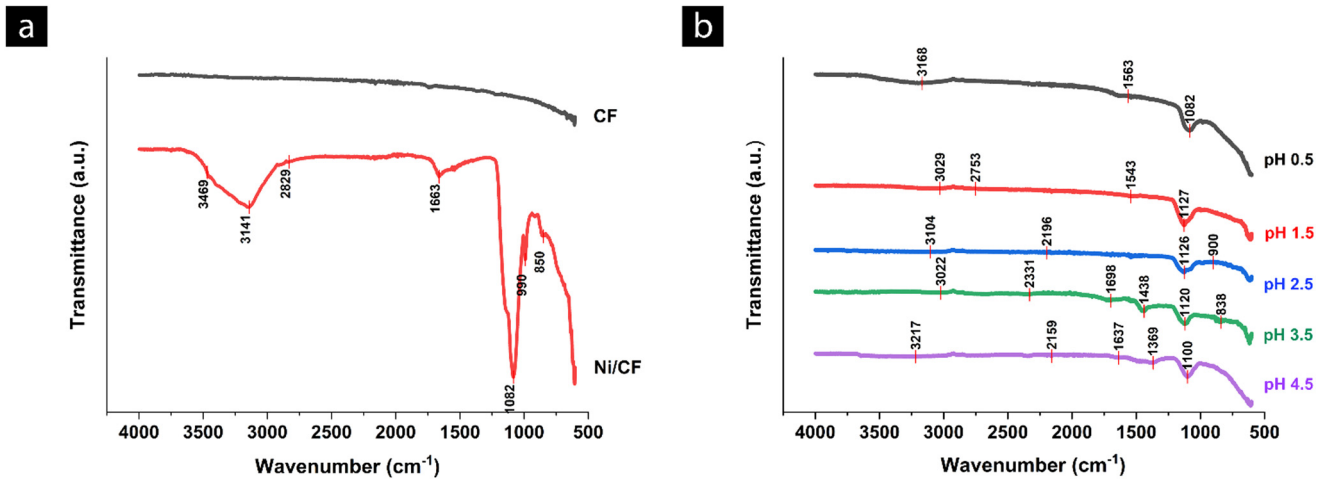

Fig. 3 a. FTIR spectra of carbon fiber (CF) and nickel-coated carbon fiber (Ni/CF). The CF spectrum shows minimal peaks, indicating a lack of significant surface functional groups. b. FTIR spectra of nickel-coated carbon fiber (Ni/CF) at different pH levels (pH-1 to pH-5). The spectra reveal variations in the presence and intensity of functional groups with changing pH.

the carbon fiber surface when exposed to strong acidic conditions associated with the acidic electrolyte (sulphuric and boric acid), in combination with the applied potential over the carbon surface which also is known to oxidize the carbon phase.[41]

Fig. 3b reveals that the pH level during the nickel coating process had smaller effects on the surface chemistry of carbon fibers. Under the most acidic conditions (pH = 1 and pH = 2), a comparatively higher presence of hydroxyl and carbonyl groups was observed around ~1100 cm^{-1}, indicating more oxidative interaction with acidic solutions. As the pH increased to neutral conditions (pH = 3 to pH = 5), there was a notable shift towards metal oxides and hydroxides (O–H groups), in agreement with the changes in the chemical environment and surface functionality with higher depositions occurring at these pH values (see section 3.1).

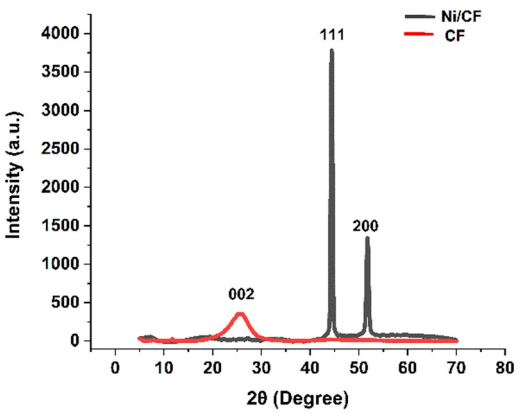

Fig. 4 XRD spectra of carbon fiber (CF) and nickel-coated carbon fiber (Ni/CF) at pH 3.5. Spectra confirms that the black spectrum, representing nickel-coated carbon fiber, shows dominant peaks for nickel at 44.5°, 51.8°, and 76.4°.

3.3 XRD analysis of electrodeposited carbon fibers

X-ray diffraction (XRD) was used to characterize the composition and structure of the coated carbon fibers. In Fig. 4, the diffraction peaks at 44.5°, 51.8°, and 76.4° confirm that nickel formation with a face-centered cubic structure was formed. The nickel diffraction peaks became more pronounced with an increased surface coverage of particles. The peak at 26.5° is characteristic of graphitic carbon (002) reflection, indicating well-ordered carbon layers in the carbon fibers. The presence of high-intensity nickel peaks on the black color spectrum confirms the successful coating of nickel on the carbon fibers, while the reduction of the carbon peak in the black spectrum (26.5°) compared to the red spectrum with the visible presence of the 002 reflections suggested that the nickel coating effectively masked the underlying carbon fiber structure. Also, no nickel oxide peaks were detected in the black spectrum obtained from the fibers coated at pH 3.5, indicating no oxide layer formed during this electrodeposition condition. The electrodeposited nickel associated with the displayed 26.5° and 44.5° peaks were in agreement with nickel deposition relationships proposed by Amblard *et al.* and corresponded to inhibited and free lateral growth of nickel, respectively.[42] The difference between the XRD and FTIR results can be explained by how each technique detects materials and their sensitivity levels. XRD is primarily sensitive to crystalline phases, and in this study, no crystalline nickel oxide phases were detected at pH 3.5, indicating that no bulk or well-ordered oxide layer formed under these conditions. In contrast, FTIR can detect both crystalline and amorphous surface species, including characteristic metal–oxygen vibrational modes. The observed FTIR shift toward metal oxide-related bands as the pH increased from 3 to 5 likely corresponds to the formation of amorphous or surface-bound nickel–oxygen species. These species are not detectable by XRD but may result from partial

Open Access Article. Published on 24 balandžio 2025. Downloaded on 2026-01-26 03:41:21.
This article is licensed under a Creative Commons Attribution 3.0 Unported Licence.

surface oxidation or nickel–oxygen coordination, consistent with electrochemical surface modifications occurring at elevated pH. Thus, the two techniques provide complementary insights into the surface chemistry and structural evolution of the system.[43,44]

3.4 UV-vis analysis of the electrolyte

Fig. 5 shows the UV-vis spectra recorded for the nickel solution from the bath before and after the electrodeposition. The spectral analysis revealed that the electrolyte bath exhibited small changes in nickel signal at the wavelengths of 395 nm and between 660–720 nm, with the execution of the electrodeposition process, *i.e.* before and after the deposition. A decrease in the intensity of the Ni^{2+} signals over time would be consistent with a reduction in the concentration of nickel ions as they are deposited onto the electrode. Importantly, this decrease in intensity occurred without any shift in the peak positions of the spectra, suggesting that the chemical environment of the nickel ions remains unchanged during the deposition process. Given the conditions (pH 3.5, 60 °C, 2 hours, 4 V), the observed changes in the UV-vis spectra were in agreement with a consumption of the Ni^{2+} ions. A small *ca.* 5% increase in transmittance at *ca.* 395 nm, with the deposition of nickel ions to the electrode, was consistent with a lower concentration of nickel ions in the electrolyte. To quantify the concentration of Ni^{2+} ions in solution before and after electrodeposition, a UV/vis calibration curve was prepared using standard nickel sulfate solutions at known concentrations. Absorbance measurements were taken at the characteristic wavelength for Ni^{2+}, and a linear calibration curve was obtained with a correlation coefficient ($R^2 > 0.99$), confirming the reliability of the method (Fig. S2†). Using this calibration curve, the Ni^{2+} concentration before electrodeposition was determined to be 1.44 g L^{-1}, while the post-electrodeposition concentration decreased to 0.672 g L^{-1}. This represents a significant reduction in nickel content and indicates effective metal ion removal through electrodeposition. In summary, the UV-vis spectra demonstrated that the electrodeposition process successfully reduced the concentration of Ni^{2+} ions in the electrolyte solution, allowing the deposition to be monitored through changes in transmittance values.

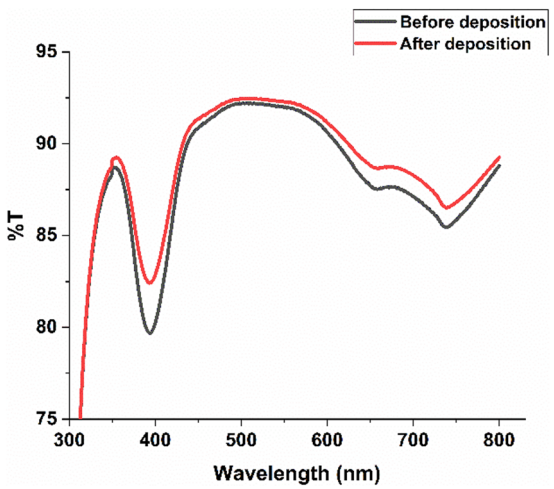

Fig. 5 UV-vis spectra for Ni^{2+} ion presence in nickel standard solution before and after 2-hour electrodeposition at pH 3.5 and 60 °C.

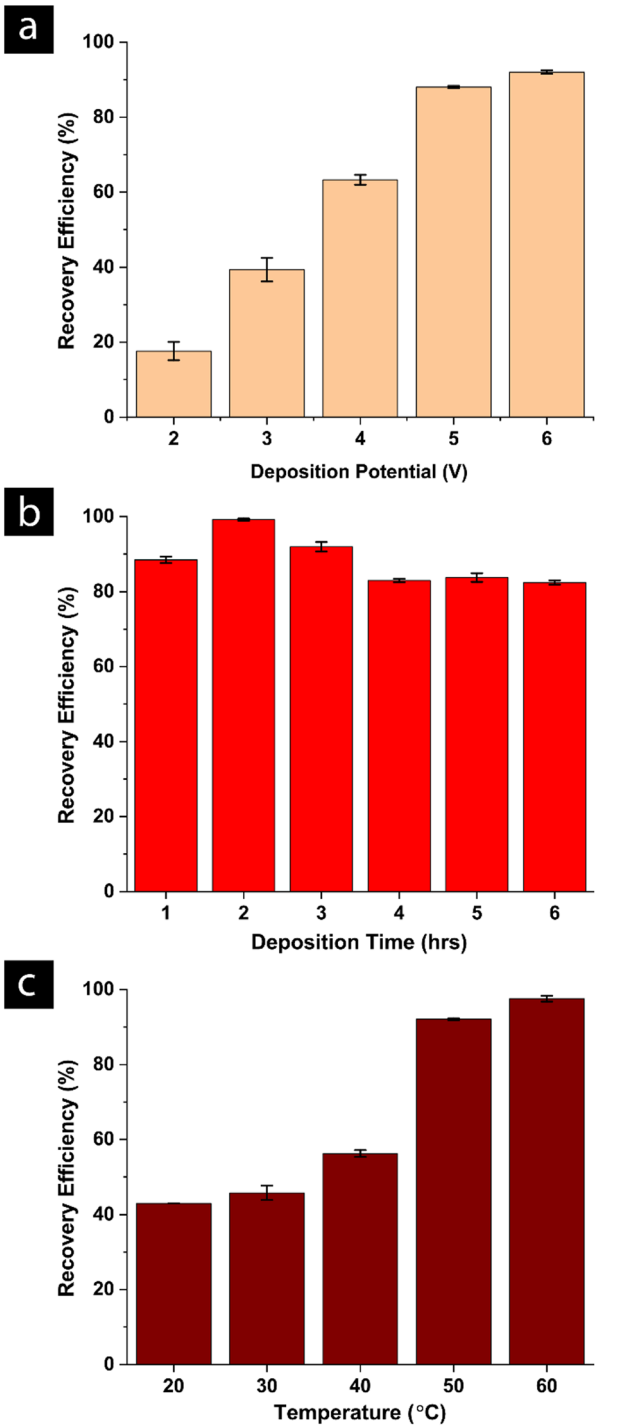

Fig. 6 a. Effect of deposition potential. b. Effect of deposition time. c. Effect of temperature.

© 2025 The Author(s). Published by the Royal Society of Chemistry

Open Access Article. Published on 24 balandžio 2025. Downloaded on 2026-01-26 03:41:21.
This article is licensed under a Creative Commons Attribution 3.0 Unported Licence.

3.5 Effect of deposition potential on recovery efficiency

The electrodeposition potential in the range of 2–6 volts was investigated, and the nickel mass recovery percentages were calculated and are shown in Fig. 6a. Within the evaluated range, the recovery rates varied from 17.6 to 92.0% recovery efficiency over the period of 2 hours at 60 °C. However, operating at an excessively high deposition potential, although providing more electrons for the reduction of Ni^{2+} ions and improving the overall recovery of nickel, has its drawbacks. For instance, a deposition potential that is too high may lead to hydrogen evolution, which competes with the nickel deposition process and can reduce current efficiency. It can also cause increased internal stress and the formation of rough or powdery deposits, compromising the quality and adherence of the nickel layer. The optimal deposition potential for maximizing nickel recovery in energy and qualitative nickel deposition characteristics was selected as 4 volts for all consecutive electrodeposition experiments. A voltage of 4.0 V was selected as it represents an optimal balance between achieving high nickel recovery efficiency and maintaining deposit quality. At this potential, a uniform and adherent nickel layer is formed with minimal co-deposition of nickel hydroxides or oxides. Furthermore, operating at 4.0 V helps to suppress excessive hydrogen evolution, which becomes more pronounced at higher voltages and can lead to increased energy consumption, reduced deposition efficiency, and poor coating adhesion.[45]

3.6 Effect of deposition time on recovery efficiency

The nature of the electrodeposits of the nickel can be associated with the changes in the electrolyte over time during the electrodeposition. The deposition time from 1 to 6 hours was therefore investigated separately for the given chemical starting conditions (at 4 volts and 60 °C), see Fig. 6b. The Ni(II) recovery percentage was 91.9% at a deposition time of 1 hour, whereas the highest nickel recovery and current efficiency were achieved at a deposition time of 2 hours. This pattern was attributed to the progressive build-up of the pure nickel layer on the electrode surface with time. However, as the deposition times increased, the electrode surface became more saturated with nickel hydroxides/oxides, resulting in higher resistance to efficient deposition. This resistance partly interfered with the deposition due to the formation of less-conductive nickel layers. Compared with results reported in the literature, the trends observed in this study are consistent with established findings, highlighting the critical balance between deposition time and recovery efficiency in optimizing electrodeposition processes.[46]

3.7 Effect of the electrolyte temperature on recovery efficiency

Fig. 6c illustrates the deposition efficiency with varying temperatures from 20 °C to 60 °C, with the nickel recovery percentages increasing as the temperature increased. The nickel recovery for 2 hours at 4 Volts was higher at 60 °C (97%) as compared to when the deposition was carried out at 20 °C (43%). The underlying reason for this temperature dependence is multifaceted, with the recovery efficiency affected in decreasing order for the following deposition parameters. An increased temperature directly affects the kinetic energy of the nickel species migrating towards the electrode surface, *i.e.* limited by their diffusion towards the electrode surface, thereby having the greatest effect on the total recovery efficiency. Although higher temperature also enhances the reduction rate of nickel ions at the carbon fiber electrode interface, this appeared not to dominantly impact the recovery efficiency since no evidence for this could be observed in Fig. 6a, *i.e.* the surface nucleation of the nickel species is significantly faster than the diffusivity and supply of the nickel species from the electrolyte. A reduced oxygen solubility, associated with the higher temperature, to some extent, may have minimized any competing oxygen reduction reactions, thereby allowing more efficient pure nickel deposition. However, a temperature increase from 20 to 60 °C, with associated oxygen dissolution values (*ca.* 10 to 5 mg L^{-1},[47] respectively), was unlikely to have influenced the deposition recovery efficiency to observed values in Fig. 6c. Furthermore, the magnitude of the oxygen-limited reduction current decreases with rising temperature, contributing to the preferential deposition of nickel over side reactions. Elevated temperatures also improve the electrolyte's conductivity, reducing the resistance within the electrochemical cell and thus increasing the overall efficiency of the electrodeposition process. These findings are consistent with the phenomena reported by Arslan *et al.* for similar effects of temperature on the electrodeposition efficiency of nickel.[48] In conclusion, in this study, the most suitable temperature for the efficient recovery of nickel was 60 °C. However, the quality of the recovered nickel was the same for all the different temperatures and formed as solid uniform layers of pure nickel.

Overall, it was evident that the total recovery efficiency highly depended on the above-reported parameters, allowing the electrolyte conditions to be optimized for the nickel metal recovery on the carbon fiber surface, resulting in a yield increase of more than 100% improvement.

3.8 Effect of pH on recovery efficiency

The solution's pH plays a critical role in the efficiency of Ni ion recovery due to its influence on the overpotential of hydrogen evolution. The pH was optimized between 0.5 and 5.5 by adjusting with varying amounts of sodium hydroxide and sulfuric acid to reach the different pHs. The optimal pH for nickel recovery was determined to be at 3.5, and recovery efficiency reached 99.3%, see Fig. 7a. At this pH, the highest current density was observed, whereas at lower current densities associated with the pH levels of 0.5 to 1.5, a recovery efficiency of 42.3 and 55.4% was reached. The more limited recovery efficiency at lower pH was explained by the increased concentration of H^+ ions available for reduction at

Open Access Article. Published on 24 balandžio 2025. Downloaded on 2026-01-26 03:41:21.
This article is licensed under a Creative Commons Attribution 3.0 Unported Licence.

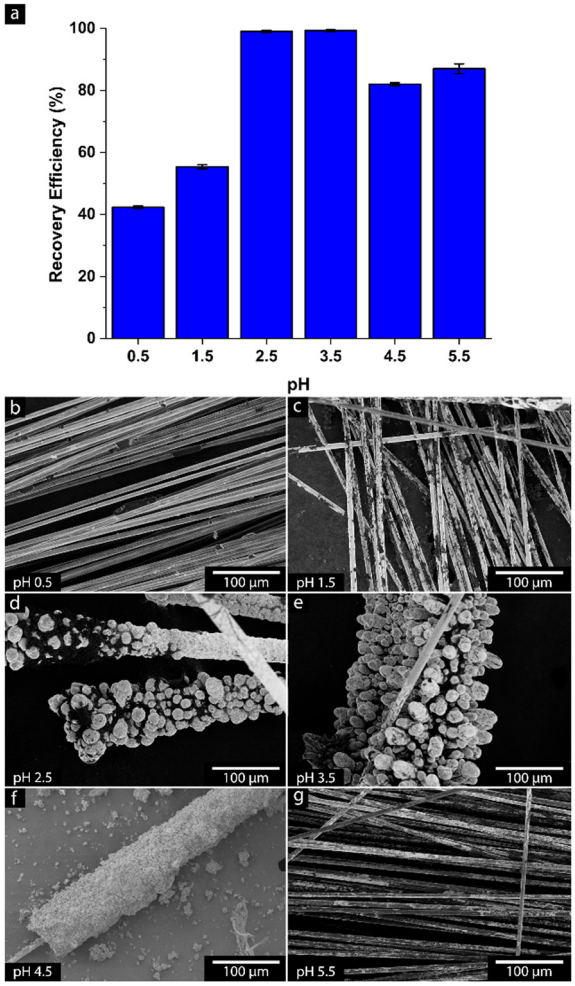

Fig. 7 a. Effect of pH on recovery efficiency b–g SEM micrographs showing the effect of pH on the morphological distribution of nickel on carbon fibers.

the cathode, competing with the Ni(II) ions for reduction, lowering both the nickel recovery and the current efficiency. On the other hand, at higher pH values, the concentration of hydroxide ions (OH^-) increases, promoting the formation of nickel hydroxide ($Ni(OH)_2$). Fig. 7a further shows that the recovery efficiency of Ni ions decreased as the pH reached levels above 3.5 due to the presence of insoluble hydroxides such as $Ni(OH)_2$ becoming more pronounced, negatively impacting the purity of the recovered nickel. The $Ni(OH)_2$ formation also adversely affected the nickel recovery by precipitating out of solution, reducing the amount of nickel available for deposition. Fig. 7b to g show the SEM micrographs for the different electrodeposition obtained at Fig. 7a, demonstrating the marked impact on the morphologies of the deposited nickel at different pHs.

At the lowest pH level, 0.5 (Fig. 7b), the nickel deposition on the carbon fibers was relatively smooth, and clean fiber surfaces were mostly hidden under an even but thin deposition of pure nickel metal. As the pH was increased to 1.5 (Fig. 7c), the even and uniform depositions remained, but due to the increased thickness, areas along the fibers with fragmented nickel can be seen. At pH 2.5 and 3.5, Fig. 7d and e, the most substantial nickel deposition occurred simultaneously as the morphologies changed to *ca.* 20 um spherical particles uniformly distributed along the fibers. Interestingly, all depositions at pH 1.5 to 3.5 were shiny silver colored, whereas those at pH 4.5 turned grey and dull. At pH 5.5, the extent and nature of the nickel deposition was almost the same as at 4.5, with powdery deposits of nickel forming along the fibers, sometimes adhering to the carbon fiber surface (Fig. 7f), while most frequently falling off as a greenish powder that didn't adhere to the carbon fiber surface, see Fig. 7g. The dominant oxygen fraction associated with the depositions at 4.5 and 5.5 are visible in Table 1, presenting the elemental analysis of coated carbon fibers at different pHs.

3.9 Mechanism for deposition

At low pH levels (0.5 to 1.5), the concentration of hydrogen ions (H^+) was high, competing with nickel ions (Ni^{2+}) for reduction at the carbon fibers. The high concentration of H^+ led to the evolution of hydrogen gas (H_2), whereas as the pH increased to 2.5, 3.5, and 4.5, and the concentration of H^+ decreased, the competition for electrons at the carbon fiber cathode favored the favorable formation of pure nickel (see reactions).

$$Ni^{2+} + 2e^{-1} \rightarrow Ni \quad (3)$$

$$2H^+ + 2e^- \rightarrow H_2 \quad (4)$$

$$Ni^{2+} + OH^- \rightarrow Ni(OH)_2 \quad (5)$$

As the competition from H^+ is decreasing (at pH 4.5 and 5.5), the nickel hydroxide $Ni(OH)_2$ formation became significant due to the higher presence of hydroxide ions (OH^-), with the formation of $Ni(OH)_2$ hindering the electrodeposition by forming a passive layer on the electrode surface, showing as the greenish powdery coatings shown in Fig. 7f and g.

3.10 Energy consumption for the nickel recovery

The energy consumption for nickel (Ni) recovery at an applied voltage of 4 volts under specific experimental conditions (initial Ni^{2+} concentration: 70 mg L^{-1}, pH 3.5, temperature: 60 °C) was comprehensively calculated to 3.6×10^{-3} kW h g^{-1} under optimized conditions (constant potential of 4 Volts, for 2 hours) according to eqn (2) (see Experimental section 2.2). This level of energy consumption is within the ranges previously reported and assumes that the electrodeposition was carried out under isothermal conditions with a continuous supply of energy to maintain the elevated temperature of the reaction bath. It can be presumed that significant energy savings could be implemented by insulating and reusing supplied energy for

© 2025 The Author(s). Published by the Royal Society of Chemistry

Open Access Article. Published on 24 balandžio 2025. Downloaded on 2026-01-26 03:41:21.
This article is licensed under a Creative Commons Attribution 3.0 Unported Licence.

better energy efficiency at the given 60 °C reaction temperature or possibly by lowering the reaction temperature. However, lowering the reaction temperature would also affect the recovery efficiency and the quality of the recycled nickel, which is not considered in eqn (2). Additional complexity in these estimations relates to the conducting nature of the carbon fiber electrode's characteristics and their surface and bulk characteristics, showing variable conductive nature depending on their initial removal of polymeric coating and performance as electrodes over the electrodepositions time when the carbon fibers have been partially coated with nickel metal or nickel metal hydroxides/oxides. It is consequently suggested that improvements in electrode material properties could markedly enhance the efficiency of Ni recovery using these flexible high surface area, strong and inexpensive carbon fibers in their large-scale future application. Akram *et al.*, which indeed achieved a much higher recovery efficiency than us, is 98.9%. However, our study emphasizes the process optimization toward energy efficiency, faster recovery, and the use of low-cost, scalable materials. While Akram *et al.* used IrO_2/Ti electrodes and a 3-hour process with 0.7 kW h g^{-1} energy consumption, our method achieved 90% recovery in just 2 hours at pH 3.5 with significantly lower energy usage (0.003 kW h g^{-1} Ni). Furthermore, the use of carbon fiber electrodes provides a more cost-effective and sustainable alternative to very costly Ir/Ti electrodes that inevitably are very expensive and challenging to scale on an industrial level.

4. Conclusions

The study reports the nickel recovery from industrial wastewater using inexpensive carbon fiber electrodes. Optimizing important parameters, including pH, temperature, deposition potential, and deposition time, enhanced the overall electrochemical nickel recovery. The solution pH was a critical factor in the process. An optimal pH of 3.5 was determined, providing the best balance for nickel recovery in terms of metal purity and quantity. At lower pH, competition between hydrogen and nickel ions for reduction hindered the effective recovery of the pure metal, whereas, at higher pH levels, significant formation of nickel hydroxides hindered the process. The temperature played a significant role in the efficiency of the nickel recovery and within the range from 30 °C to 60 °C, deposition at 60 °C allowed for improved recovery rates due to increased kinetic energy of the deposited nickel species, facilitating faster electrochemical reactions. Moreover, the elevated temperatures decreased the solubility of oxygen in the electrolyte, thereby reducing competing oxygen reduction reactions and promoting more efficient nickel deposition. An optimal deposition potential of 4 volts was determined, providing sufficient electrons to reduce nickel ions while avoiding excessive hydrogen evolution, which could interfere with nickel deposition. This potential increased the nucleation rate of nickel on the electrode surface, resulting in a more uniform and dense nickel layer, thus improving the recovery deposition nature. Extending the deposition time beyond 2 hours resulted in a more limited recovery efficiency due to increased electrode resistance, explained by the formation of unpure nickel deposits. This suggests that timely field reversal can be advantageous. The optimized conditions demonstrated in this research provide a practical and viable method for nickel recovery from mining wastewater. This approach contributes to environmental protection by mitigating nickel pollution and supports resource sustainability by recovering valuable metals from wastewater. The results ensure better environmental management and compliance with regulatory standards, presenting a significant advancement in wastewater treatment and resource recovery.

Data availability

All relevant data are included in the manuscript.

Author contributions

AP, KT, and PRD carried out the experiments. AB assisted with all the manuscript preparation and provided scientific feedback. AP wrote the manuscript with RTO, assisted by AB, BKB, RA, KT, and AB. BKB assisted with microscopic analysis. RA, SA, and SS assisted with industrial feedback and information on environmental policies concerning wastewater. All authors reviewed the manuscript and approved its content.

Conflicts of interest

There are no conflicts of interest to declare.

Acknowledgements

All the authors wish to acknowledge Vinnova for financing the EcinRaw project (2021-03738) and Wallenberg Initiative Materials Science for Sustainability (WISE), funded by the Knut and Alice Wallenberg Foundation.

References

1 G. S. Simate and S. Ndlovu, *J. Environ. Chem. Eng.*, 2014, **2**, 1785–1803.
2 A. Akcil and S. Koldas, *J. Cleaner Prod.*, 2006, **14**, 1139–1145.
3 F. Fu and Q. Wang, *J. Environ. Manage.*, 2011, **92**, 407–418.
4 J. Chen, C. Tang, Y. Sakura, J. Yu and Y. Fukushima, *Hydrogeol. J.*, 2005, **13**, 481–492.
5 *Heavy Metals in Soils: Trace Metals and Metalloids in Soils and Their Bioavailability*, ed. B. J. Alloway, Environmental Pollution, Springer, Dordrecht, 2012, vol. 22, pp. 11–50.
6 G. Tóth, T. Hermann, M. R. Da Silva and L. Montanarella, *Environ. Int.*, 2016, **88**, 299–309.

Open Access Article. Published on 24 balandžio 2025. Downloaded on 2026-01-26 03:41:21.
This article is licensed under a Creative Commons Attribution 3.0 Unported Licence.

7 B. Zambelli and S. Ciurli, Nickel and Human Health, in *Interrelations between Essential Metal Ions and Human Diseases*, ed. A. Sigel, H. Sigel and R. Sigel, Metal Ions in Life Sciences, Springer, Dordrecht, 2013, vol. 13.
8 C. K. Jain, D. S. Malik and A. K. Yadav, *Environ. Process*, 2016, **3**, 495–523.
9 N. Efaq, A. Al-Gheethi, R. M. S. Radin Mohamed, M. Al-Sahari, M. S. Hossain, D.-V. N. Vo and M. Naushad, *Chemosphere*, 2022, **291**, 132862.
10 J. Zagorc-Koncan and M. Cotman, *Water Sci. Technol.*, 1996, **34**, 141–145.
11 M. Rizwan, K. Usman and M. Alsafran, *Chemosphere*, 2024, **357**, 14202.
12 X. Li and I. Thornton, *Appl. Geochem.*, 2001, **16**(14), 1693–1706.
13 S. Buxton, E. Garman, K. E. Heim, T. Lyons-Darden, C. E. Schlekat, M. D. Taylor and A. R. Oller, *Inorganics*, 2019, **7**, 89.
14 M. Rizwan, K. Usman and M. Alsafran, *Chemosphere*, 2024, **357**, 142028.
15 S. S. Kolluru, S. Agarwal, S. Sireesha, I. Sreedhar and S. R. Kale, *Process Saf. Environ. Prot.*, 2021, **150**, 323–355.
16 G. Tchobanoglous, F. L. Burton and H. D. Stensel, *Wastewater Engineering, Treatment and Reuse*, Metcalf & Eddy Inc., McGraw-Hill, 4th edn, 2003.
17 *Physicochemical Treatment Processes*, ed. L. K. Wang, N. K. Shammas and Y. T. Hung, Handbook of Environmental Engineering, Springer Science & Business Media, 2010.
18 P. R. Rout, T. C. Zhang, P. Bhunia and R. Y. Surampalli, *Sci. Total Environ.*, 2021, **753**, 141990.
19 World Health Organization (WHO), Geneva, 2011.
20 É. Lèbre, G. D. Corder and A. Golev, *Miner. Eng.*, 2017, **107**, 34–42.
21 C. Vischetti, E. Marini, C. Casucci and A. De Bernardi, *Environments*, 2022, **9**, 133.
22 G. Tóth, T. Hermann, M. R. da Silva and L. Montanarella, *Environ. Int.*, 2016, **88**, 299–309.
23 V. Kumar Parida, D. Saidulu, A. Majumder, A. Srivastava, B. Gupta and A. K. Gupta, *J. Environ. Chem. Eng.*, 2021, **9**, 105966.
24 A. Abidli, Y. Huang, Z. Ben Rejeb, A. Zaoui and C. B. Park, *Chemosphere*, 2022, **292**, 133102.
25 T. M. Mokgehle and N. T. Tavengwa, *Appl. Water Sci.*, 2021, **11**, 42.
26 European Commission, **https://ec.europa.eu/environment/water/water-dangersub/industrial_en.htm**.
27 B. Zhou, X. Zhang, P. Wang, X. Zhang, C. Wei, Y. Wang and G. Wen, *J. Mol. Liq.*, 2024, **401**, 124644.
28 H. N. Tran, S.-J. You, A. Hosseini-Bandegharaei and H.-P. Chao, *Environ. Res.*, 2023, **203**, 111861.
29 W. Brostow and H. E. Hagg Lobland, *Materials: Introduction and Applications*, Chapter: Materials Recycling and Sustainability, John Wiley & Sons, 2017, pp. 437–438.
30 M. Yu, E. Budiyanto and H. Tüysüz, *Angew. Chem., Int. Ed.*, 2022, **61**, e202103824.
31 M. Nicol, N. Welham and G. Senanayake, *Hydrometal.*, 2022, pp. 271–393.
32 U. Ulissi and R. Raccichini, *Front. Nanosci.*, 2021, **19**, 1–28.
33 Z. Rao, S. J. Hearne and E. Chason, *J. Electrochem. Soc.*, 2019, **166**, D3212.
34 T. R. Koenig, Z. Rao, E. Chason, G. J. Tucker and G. B. Thompson, *Surf. Coat. Technol.*, 2021, **412**, 126973.
35 S. Awasthi, S. De and S. K. Pandey, *Heliyon*, 2024, **10**, e26051.
36 W. Wu, D. Xie, J. Huang, Q. Wang, Q. Chen and J. Huang, *J. Adhes.*, 2022, **99**, 1099–1122.
37 A. Lelevic and F. C. Walsh, *Surf. Coat. Technol.*, 2019, **369**, 198–220.
38 N. Ostojic, Z. Duan, A. Galyamova, G. Henkelman and R. M. Crooks, *J. Am. Chem. Soc.*, 2018, **140**, 13775–13785.
39 A. Lelevic and F. C. Walsh, *Surf. Coat. Technol.*, 2019, **378**, 124803.
40 A. M. Pourrahimi, R. L. Andersson, K. Tjus, V. Ström, A. Björk and R. T. Olsson, *Sustainable Energy Fuels*, 2019, **3**, 2111–2124.
41 S. Li, Y. Jin, Z. Wang, Q. He, R. Chen, J. Wang, H. Wu, X. Zhao and J. Mu, *Colloid Polym. Sci.*, 2019, **297**, 967–977.
42 J. Amblard, I. Epelboin, M. Froment and G. Maurin, *J. Appl. Electrochem.*, 1979, **9**, 233–242.
43 S. Pasieczna-Patkowska, M. Cichy and J. Flieger, *Molecules*, 2025, **30**, 684.
44 A. M. Holder and R. E. Schaak, *ACS Nano*, 2019, **13**, 7359–7365.
45 A. Yavuz, N. Ozdemir, P. Yilmaz Erdogan, H. Zengin, G. Zengin and M. Bedir, *Thin Solid Films*, 2020, **711**, 138309.
46 M. Akram, Z. Bano, S. U. A. Bhutto, J. Pan, A. Uddin, M. Z. Afzal, L. Li, M. Xia and F. Wang, *J. Environ. Chem. Eng.*, 2024, **12**, 112830.
47 R. F. Weiss, *Deep-Sea Res.*, 1970, **17**, 721–773.
48 O. G. Arslan, C. Bombach and H. Stelter, *Hydrometallurgy*, 2002, **65**, 1–8.

© 2025 The Author(s). Published by the Royal Society of Chemistry